ACS APPLIED MATERIALS & INTERFACES

Research Article

www.acsami.org

Hemin-Block Copolymer Micelle as an Artificial Peroxidase and Its Applications in Chromogenic Detection and Biocatalysis

Rui Qu,[†] Liangliang Shen,[†] Zhihua Chai,[†] Chen Jing,[†] Yufeng Zhang,*[,‡] Yingli An,[†] and Linqi Shi*[,†]

[†]State Key Laboratory of Medicinal Chemical Biology, Key Laboratory of Functional Polymer Materials, Ministry of Education, Institute of Polymer Chemistry, Collaborative Innovation Center of Chemical Science and Engineering (Tianjin), Nankai University, Tianjin 300071, China

[‡]State Key Laboratory of Hollow Fiber Membrane Materials and Processes, Tianjin Polytechnic University, Tianjin 300387, China

Supporting Information

ABSTRACT: Following an inspiration from the fine structure of natural peroxidases, such as horseradish peroxidase (HRP), an artificial peroxidase was constructed through the self-assembly of diblock copolymers and hemin, which formed a functional micelle with peroxidase-like activity. The pyridine moiety in block copolymer poly(ethylene glycol)-*block*-poly(4-vinylpyridine) (PEG-*b*-P4VP) can coordinate with hemin, and thus hemin is present in a five-coordinate complex with an open site for binding substrates, which mimics the microenvironment of heme in natural peroxidases. The amphiphilic core−shell structure of the micelle and the coordination interaction of the polymer to the hemin inhibit the formation of hemin μ-oxo dimers, and thereby enhance the stability of hemin in the water phase. Hemin-micelles exhibited excellent catalytic performance in the oxidation of phenolic and azo compounds by H_2O_2. In comparison with natural peroxidases, hemin-micelles have higher catalytic activity and better stability over wide temperature and pH ranges. Hemin-micelles can be used as a detection system for H_2O_2 with chromogenic substrates, and they anticipate the possibility of constructing new biocatalysts tailored to specific functions.

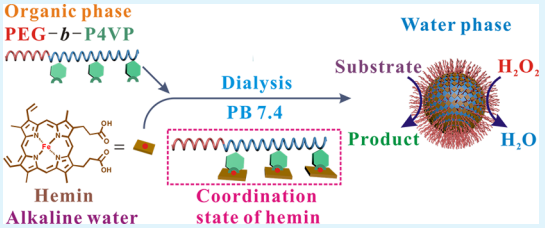

KEYWORDS: *hemin, block copolymer, micelle, coordination, artificial peroxidase*

1. INTRODUCTION

Enzymes are extremely efficient at catalyzing a variety of reactions with high substrate specificity, activities, and yields under mild reaction conditions.[1] Because of these advantages, enzymes have been widely applied as biological catalysts in environmental, industrial, medical, and biosensing fields. However, the disadvantages of natural enzymes cannot be ignored, for example, their low operational stability, high cost, high sensitivity to the environment, and recovery and recycling difficulties, which may limit their further applications. Therefore, the development of artificial enzymes that can overcome the disadvantages of natural enzymes are highly desired.[2] Many attempts have been made to construct artificial enzymes to copy or even surpass the functions of natural enzymes. Artificial enzymes are based on the principles of enzyme action, such as the initial binding interaction between the substrate and the enzyme, the activation of the bound substrate by properly positioned catalytic groups, and transition-state stabilization.[3] Generally, even simple metal complexes can act as enzyme mimics, and more sophisticated supramolecular structures endow the catalytic center with preferable stability and continuous activity.[4] By employing the principles of enzyme action and the advantages of supramolecular chemistry, a number of supramolecular artificial enzymes were prepared on the basis of various supramolecular materials including macrocycles (such as cyclodextrins and calixarenes), container molecules (such as cavitands and capsules), self-assembled nanometer-sized objects (for example, micelles, vesicles, nanoparticles, nanotubes, and nanogels) and others.[5]

Peroxidases form a large family of enzymes that catalyze oxidation reactions with hydrogen peroxide (H_2O_2) or alkyl peroxide. Horseradish peroxidase (HRP) is an important heme-containing peroxidase, and it employs an α-helical protein binding heme as a cofactor.[6] Heme is a ferrous porphyrin, and it acts as the catalytic active center of HRP. The peptide chains in HRP create a hydrophobic microenvironment for heme, and they also provide some important amino acid residues, such as histidines, which may improve the catalytic activity and efficiency of heme. In aqueous media, the hydrophobic interaction of heme with polypeptides and the coordination interaction of histidine to heme are both important for creating a stable conjugate.[7] Heme-containing peroxidases are currently used for a wide range of applications such as electrochemical sensors, wastewater treatment and immunohistochemistry.[6] With inspiration from the structures of natural peroxidases, much attention has been devoted to mimicking peroxidase. Efforts to produce heme-containing artificial peroxidase are focused on the design of the scaffolds, carbon nanotubes,[8]

Received: August 5, 2014
Accepted: October 6, 2014
Published: October 6, 2014

synthetic peptides,[9] nanosheets of Fe−Ni layered double hydroxide,[10] graphene hybrid nanosheets[11,12] and supramolecular hydrogel[13] were all confirmed to be excellent scaffolds for heme; they successfully achieved the deaggregation and stable dispersion of heme in a specific medium. It is difficult for heme to maintain high catalytic activity in aqueous media because of its low solubility and high tendency to form μ-oxo dimers or self-aggregate. Despite these problems, it is necessary to transition the peroxidase mimics from the organic phase to the water phase because of their wide range of applications in biochemistry. Scolaro et al. reported an artificial peroxidase that was soluble in aqueous solution. An acid−base interaction between hemin and poly(amidoamine) (PAMAM) dendrimers provides the supramolecular noncovalent peroxidase systems. These dendrimers provide a charged scaffold that effectively prevents hemin from aggregating or forming μ-oxo dimers.[14] Dong et al. reported a novel polypyrrole/hemin nanocomposite that was prepared by combining a pyrrole monomer with a hemin molecule through chemical oxidation polymerization. The resulting nanocomposite was well dispersed in aqueous solution with the help of an effective surfactant, and it exhibited intrinsic peroxidase-like catalytic activities.[15] In addition to its stability in aqueous solution, another point should be mentioned that has long been neglected when building artificial peroxidases, which is the peptidic microenvironment of heme. Xu et al. reported on a hydrogel nanoenzyme model of peptide nanofiber, which they made by mixing hemin and histidine into molecular hydrogel as formed by the self-assembly of two derivatives of amino acids. These supramolecular hydrogels protect monomeric hemin by preventing degradation and dimerization, and they facilitate the catalytic process by providing nanoporous diffusion channels, which allows substrate transport.[13] The hydrogel network and amino acid residues provide a microenvironment for the artificial peroxidase that is similar to that of the natural enzyme. Based on an analysis of previous studies, an ideal heme carrier should provide an inner hydrophobic environment and an outer hydrophilic scaffold, which can simultaneously stabilize heme in aqueous media and inhibit its aggregation. In addition, the carrier should contain histidine residues or analogs, which can provide the necessary coordinating groups for heme to achieve specific functions.

Polymeric assemblies can serve as excellent carriers for some functional chemicals because of their high stability in aqueous media. The micelle, which is the most common form of polymeric assemblies, has a hydrophobic core that can load some hydrophobic biomolecules, and it has a hydrophilic shell that can stabilize the system in aqueous media.[16,17] The structure of the micelle is similar to that of the structural organization of globular proteins. Until the present, many functional micelles containing biomolecules have been constructed; however, it is rare to see micelles used as a platform to develop artificial enzymes with peroxidase-like activity and a similar microenvironment.[18−21] Our research group has long been devoted to cooperative macromolecular self-assembly toward polymeric assemblies with multiple and bioactive functions.[22] Thus, we are trying to build an artificial peroxidase through the self-assembly of diblock copolymers and hemin, which forms a functional micelle with peroxidase-like activity, as shown in Scheme 1. The hemin-micelle exhibited excellent catalytic activity during the oxidation of phenolic compounds and azo-compounds in which H_2O_2 acted as the oxidant. In comparison with natural peroxidase, the artificial peroxidase constructed by self-assembling a block copolymer and hemin exhibited higher catalytic activity and better stability. In addition, the hemin-micelle is easy to prepare and preserve, and its cost is much lower than that of natural peroxidases. The artificial peroxidase constructed from hemin-micelles can be used as a detection system for H_2O_2 and as biocatalysts tailored to specific functions.

Scheme 1. Schematic Illustration of the Formation of the Hemin-Micelle and Catalytic Process

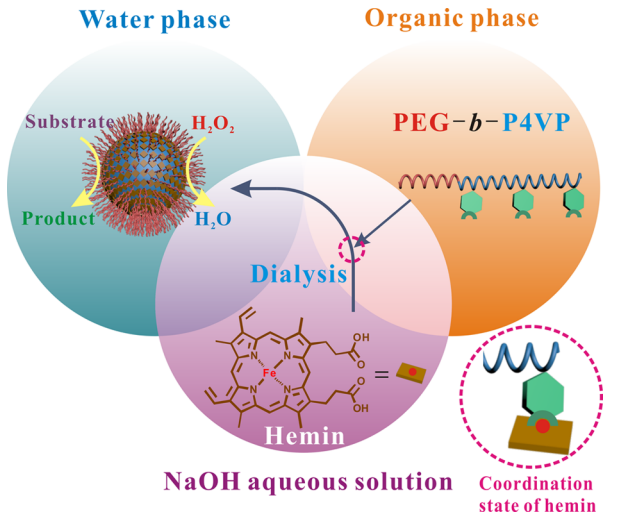

2. MATERIALS AND METHODS

2.1. Materials. Poly(ethylene glycol) monomethyl ether (CH_3O-PEG_{45}−OH) (M_n = 2000 g/mol) was purchased from Fluka. CuCl and 4-vinylpyridine were purchased from Sigma-Aldrich and purified according to ref 23. Tris [2-(dimethylamino) ethyl] amine (Me_6TREN) was synthesized according to ref 23. Hemin (98%) was purchased from Energy Chemical (Shanghai, China). Orange II (an analytical standard) and 3, 3′, 5, 5′-tetramethylbenzidine (98%) were purchased from Heowns Business License (Tianjin, China). Catechol (99%), ε-(benzyloxycarbonyl)-L-lysine (98%) and ε-caprolactone (99%) were purchased from J&K Chemical Company (Beijing, China). Stannous octoate ($Sn(Oct)_2$) (96%) was purchased from Alfa Aesar. Horseradish peroxidase (HRP) (250 U/mg) was purchased from Sanland. All the reagents were used without further purification. All aqueous solutions were prepared with ultrapure water (>18 MΩ) from a Millipore Mill-Q system.

2.2. Apparatus. ^{1}H NMR spectra were recorded on a Varian UNITY-plus 400 M NMR spectrometer at room temperature with tetramethylsilane (TMS) as an internal standard. The number-average molecular weight (M_n) and weight-average molecular weight (M_w) were measured by gel permeation chromatography (GPC) at 25 °C with a Waters 1525 chromatograph equipped with a Waters 2414 refractive index detector. GPC measurements were performed by using THF as eluents with a flow rate of 1.0 mL/min. Dynamic laser scattering (DLS) measurements were performed with a laser light scattering spectrometer (BI-200SM) equipped with a digital correlator (BI-9000AT) at 532 nm. All samples were prepared by filtering approximately 1 mL of solution through a 0.45 μm Millipore filter into a clean scintillation vial and then characterizing them at 25 °C. The zeta potential values were measured on a Brookheaven ZetaPALS (Brookheaven Instrument, USA). This instrument employs phase analysis light scattering at 25 °C to provide an average over multiple particles. Transmission electron microscopy (TEM) measurements were performed with a commercial Philips T20ST electron microscope at an acceleration voltage of 200 kV. UV−vis absorption spectra were measured on a UV-2550 UV−vis spectrophotometer (Shimadzu, Japan).

2.3. Synthesis and Characterization of Diblock Copolymers. The block copolymers poly(ethylene glycol)-*block*-poly(4-vinylpyridine) (PEG-*b*-P4VP), poly(ethylene glycol)-*block*-poly(L-lysine) (PEG-*b*-PLys) and poly(ethylene glycol)-*block*-poly(ε-caprolactone) (PEG-*b*-PCL) were synthesized according to refs 24 25, and 26, respectively. The polymer synthesis routes and characterizations are shown in the Supporting Information.

2.4. Preparing Hemin/Block Copolymer Micelles. *2.4.1. Hemin/PEG-b-P4VP Micelles.* The hemin stock solution (100 μg/mL) was prepared in NaOH solution (0.2 M) and vigorously stirred for 12 h. The block copolymer PEG_{45}-*b*-$P4VP_{145}$ was dissolved in anhydrous N,N-Dimethylformamide (DMF). The desired volume of polymer solution was added dropwise to the hemin solution under vigorous stirring. When the addition was finished, the stirring was continued for another 12 h, followed by dialysis against 10 mM phosphate buffer (pH 7.4) for 24 h to remove the free hemin that was not loaded on the micelle and to adjust the pH to neutral. The mass ratio of PEG-*b*-P4VP to hemin (defined as *R*) was varied from 0.5 to 4 by changing the volume of the polymer solution, which was added to the same amount of hemin stock solution.

2.4.2. Hemin/PEG-b-PLys Micelles. The block copolymer PEG_{114}-*b*-$PLys_{50}$ was dissolved in neutral water. The desired volume of polymer solution was added to the hemin solution (100 μg/mL in 0.2 M NaOH solution) under vigorous stirring, followed by dialysis against 10 mM phosphate buffer (pH 7.4) for 24 h, to adjust the pH to neutral.

2.4.3. Hemin/PEG-b-PCL Micelles. The block copolymer PEG_{114}-*b*-PCL_{42} was dissolved in anhydrous DMF. The desired volume of polymer solution was added dropwise to the hemin solution (100 μg/mL in 0.2 M NaOH solution) under vigorous stirring, and when the addition was finished, stirring was continued for another 12 h, followed by dialysis against 10 mM phosphate buffer (pH 7.4) for 24 h to remove the DMF and adjust the pH to neutral.

2.5. Catalytic Dynamics Study. The Orange II solution (0.25 mM in 10 mM phosphate buffer pH 7.4) was mixed with the same volume of H_2O_2 solution (6.85 mM in 10 mM phosphate buffer pH 7.4) and hemin-micelles (with varied concentrations of hemin from 12.5 μg/mL to 100 μg/mL) at different pH values and temperatures. The catalytic dynamics experiments were performed in time course mode by monitoring the absorbance change at 484 nm, which was the characteristic absorption peak of the Orange II substrate on the UV−vis spectrophotometer.

The molar absorption coefficient (ε_{484} nm) of Orange II at 484 nm was calculated by using a serious of standard curves at varied temperatures. The initial rate of the reaction can be obtained by using the following equation

$$\Delta c = \frac{\Delta \mathrm{Abs}}{\varepsilon b} \tag{1}$$

$$v = \frac{\Delta c}{\Delta t} \tag{2}$$

where Abs is the intensity of the absorption peak, ε is the molar absorption coefficient, b is the optical path (the light transmittance thickness of cuvette), c is the concentration of the substrate, t is time, and v is the initial rate.

The Michaelis−Menten constant (K_m) and maximum initial velocity (V_{max}) were determined by using the Lineweaver−Burk model, which is the double reciprocal of the Michaelis−Menten equation. The data were analyzed by using the following equation

$$\frac{1}{v} = K_m/V_{max}\left(\frac{1}{[S]} + \frac{1}{K_m}\right) \tag{3}$$

where v is the initial rate and [S] is the substrate concentration. The initial rates at different substrate concentrations were measured, and the K_m and V_{max} can be obtained by making a linear fit between the reciprocals of v and [S].

The percentage conversion (Y) can be obtained by using the following equation:

$$Y = \left(\frac{A_0 - A_{60}}{A_0}\right)100 \tag{4}$$

where A_0 is the absorbance at time zero and A_{60} is the absorbance after 60 min of reaction.

The catalytic reaction in which HRP was a catalyst was also performed. HRP stock solutions at different concentrations were obtained by dissolving the desired volume of HRP in 10 mM phosphate buffer (pH 7.4), and stored at 4 °C.

2.6. Chromogenic H_2O_2 Tests with TMB and Catechol. Chromogenic tests of H_2O_2 were performed with two different substrates, namely 3, 3′, 5, 5′-tetramethylbenzidine (TMB) and catechol. The TMB solution (0.5 mM in 0.2 mM NaAc-HAc buffer, pH 4.0) was mixed with the same volume of H_2O_2 solution (6.85 mM in 10 mM phosphate buffer pH 7.4). Hemin-micelles (100 μg/mL hemin in 10 mM phosphate buffer pH 7.4) at the same volume as the TMB solution were added to the TMB and H_2O_2 mixture. The characteristic absorption peak of oxyTMB at 652 nm was measured by using UV−vis spectra. The color change was captured on the camera. With regards to catechol, the detection solution was prepared by mixing the same volume of catechol solution (0.25 mM in 10 mM phosphate buffer pH 7.4) and hemin-micelles (100 μg/mL hemin in 10 mM phosphate buffer pH 7.4). Dilute H_2O_2 solution (30 mM in 10 mM phosphate buffer pH 7.4) was added dropwise to the detection solution. The color change in the detection solution could be observed in less than 1 min. UV−vis spectra were recorded every 2 min to detect changes in the characteristic peaks.

3. RESULTS AND DISCUSSION

3.1. Micellization of PEG-*b*-P4VP and Hemin. Several amino acids are known to serve as axial or proximal ligands to heme proteins. Histidine, tyrosine, cysteine and lysine are common axial ligands that coordinate heme. Peroxidases, such as horseradish peroxidase and cytochrome c peroxidase, are five-coordinate compounds with an open site for binding small molecules such as H_2O_2 and some other substrates. In these peroxidases, histidine is the axial ligand and can facilitate proton transfer by promoting the formation of a hydrogen bond in the catalytic center of the enzymes, which plays important roles in modulating the structure and catalytic property.[27,28] In our previous investigation, poly(ethylene glycol)-*block*-poly(4-vinylpyridine) (PEG-*b*-P4VP) has long been used as a block copolymer to protect and stabilize metalloporphyrins in aqueous media because of its excellent amphipathicity and high coordination ability.[24,29−31] The micelle was formed with a hydrophilic PEG shell and a hydrophobic P4VP core, which can be used as a supramolecular scaffold for some hydrophobic biomolecules. In addition, the pyridine moiety in the P4VP chain was an excellent substitute for the imidazole moiety in the histidine, which can coordinate with heme and offer a similar microenvironment to that of the histidine residue in heme proteins.[32,33] Thus, PEG-*b*-P4VP was used to build the scaffold for the hemin, which was expected to mimic the heme microenvironment in natural peroxidases.

Hemin is difficult to dissolve in acidic and neutral aqueous media, and it also has poor solubility in most organic solvents. In alkaline water, it has relatively good solubility because of the two carboxy groups on the hemin. The pK_a of P4VP is 4.5−4.7, which makes it insoluble in neutral and alkaline aqueous media.[34] It was difficult to dissolve the two components in the same phase because of the large difference in their solubilities, which increased the difficulty of self-assembly. We skillfully adopted a two-phase method to prepare the micelle. The PEG-*b*-P4VP that was dissolved in DMF was added dropwise to the hemin/NaOH solution, the P4VP block was strongly hydro-

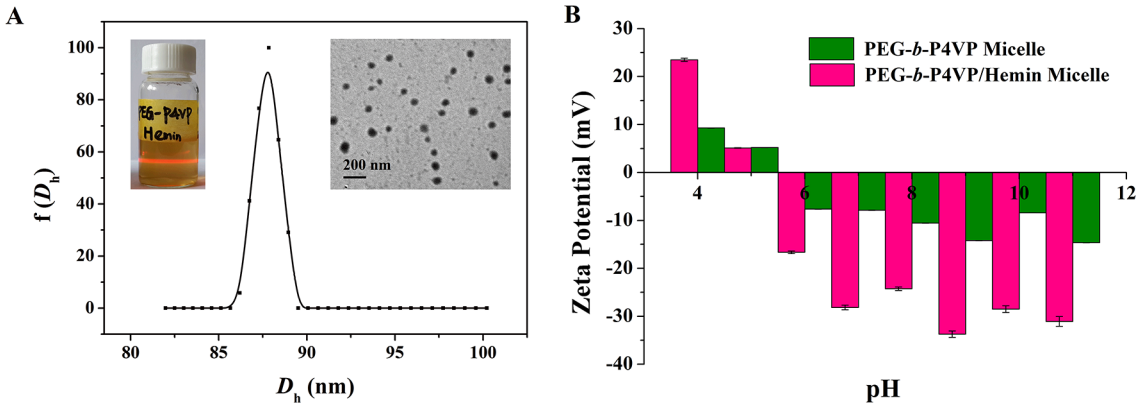

Figure 1. (A) Hydrodynamic diameter distribution of the hemin-micelle in aqueous solution. Inset: the photograph (left) and TEM image (right) of the hemin-micelle. Laser light (inset, left) was obtained by using a simple laser generator (650 nm, 5 mW). (B) Zeta potentials of the PEG-*b*-P4VP micelle and PEG-*b*-P4VP/hemin micelle at various pH values at 25 °C.

phobic in alkaline solution and formed the hydrophobic core, and the hydrophilic PEG chain dispersed around the core to stabilize the system in aqueous media. The pyridine group in P4VP can coordinate with the iron in the hemin core, and thus the hemin was loaded on the P4VP core. The PEG chains along with the P4VP-hemin core can act as protein pockets in natural peroxidase, which brings about a special inclusion behavior between the catalyst and the substrate. When the pH changes from alkaline to neutral, the ionization degree of the carboxy groups became smaller and hemin became more hydrophobic, which made the structure of P4VP-hemin core more compact.

Figure 1A shows the hydrodynamic diameter distribution f (D_h) and the TEM image of hemin-micelles with R (mass ratio of PEG-*b*-P4VP to hemin) = 1. The DLS result indicates that the micelle is reasonably monodisperse, and the average D_h is approximately 88 nm. A TEM micrograph of the micelle revealed that the hemin-micelle is a spherical particle, and the diameter distribution of the micelle is approximately 60−80 nm. The D_h of the micelle as measured by DLS is larger than that observed by TEM because the micelle became swollen in water, whereas the TEM measurements were performed with dried samples.

The surface structure of the micelle can be confirmed by zeta potential analysis (Figure 1B). When the pH is above 5, the hemin-micelle carries a clear negative charge. At a higher pH, the absolute value of the charge remains at a high level, which is much higher than that of the PEG-*b*-P4VP micelle without loading hemin. The excess charge is attributed to the carboxy groups of the hemin, which supports the idea that the hemin is successfully loaded on the micelle.

3.2. Coordination Properties of Hemin-Micelles. The coordination interaction was the primary driving force for loading hemin on to the P4VP core and further self-assembling it into a micelle, which greatly increased the stability of the hemin in aqueous media. Figure 2 shows the UV−vis spectra of hemin in alkaline solution (0.2 M NaOH solution) and in the micelle (pH 7.4). The free hemin in alkaline solution displays a Soret peak at 390 nm along with a shoulder at 365 nm, which indicates the presence of a mixture of the hemin dimer connected by μ-oxo bridges (μ-oxo dimer) and the monomeric hemin hydroxide. In addition, a low-intensity band at 610 nm is consistent with the Q-band value of the μ-oxo dimer.[13,35] Therefore, the primary structures of hemin in alkaline solution are the μ-oxo dimers and a small amount of hematins. The presence of the μ-oxo dimer is unfavorable for the stability of

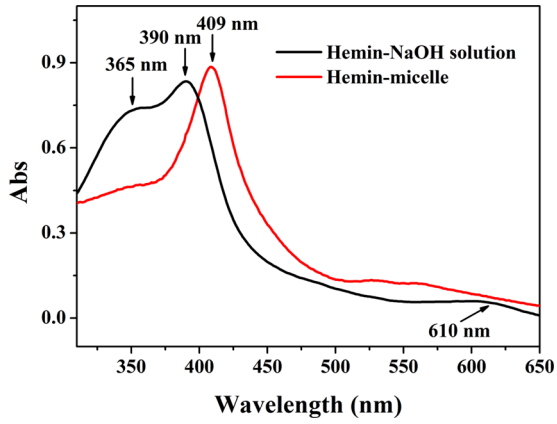

Figure 2. UV−vis spectra of free hemin in 0.2 M NaOH aqueous solution and hemin in the micelle (pH 7.4).

hemin in water, and it further influences the catalytic activity of hemin. The Soret band of the hemin-micelle (409 nm) has a red shift compared with that of monomeric hemin (approximately 400 nm).[36] The red shift is attributed to the coordination interaction between the pyridine and the hemin, and the Soret band of the hemin-micelle (409 nm) was similar to that of the hemin-histidine complex.[13,36] The analysis above demonstrates that there are no μ-oxo dimers of hemin in the hemin-micelle, and the low hemin concentration and the coordination interaction between the pyridine and the hemin inhibit the formation of the μ-oxo dimer.[9]

3.3. Catalytic Activity and Catalytic Dynamics. The peroxidase-like activity of the hemin-micelle was assessed by using Orange II and H_2O_2 as substrates. Orange II has one of the simplest azo dye structures and has served as a model dye for testing many biological and chemical treatments.[37−39] The azo structure can be destroyed by H_2O_2 with peroxidase as a catalyst, as shown in Scheme 2. The proposed mechanism for the reaction is shown in the Supporting Information. The decreased absorbance caused by the decomposition of Orange II was monitored by UV−vis spectrophotometer at 484 nm. Figure 3 A shows the change in the UV−vis spectra along with the reaction. In the absence of H_2O_2 or hemin-micelles, the spectra remained unchanged. The absorption peak at 484 nm decreased rapidly in the case of H_2O_2, Orange II and hemin-micelles, which indicated the degradation of Orange II.

Scheme 2. Degradation of Orange II by H_2O_2 with HRP as a Catalyst

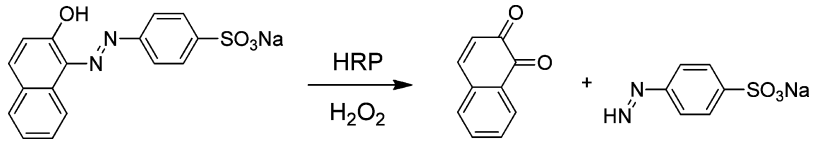

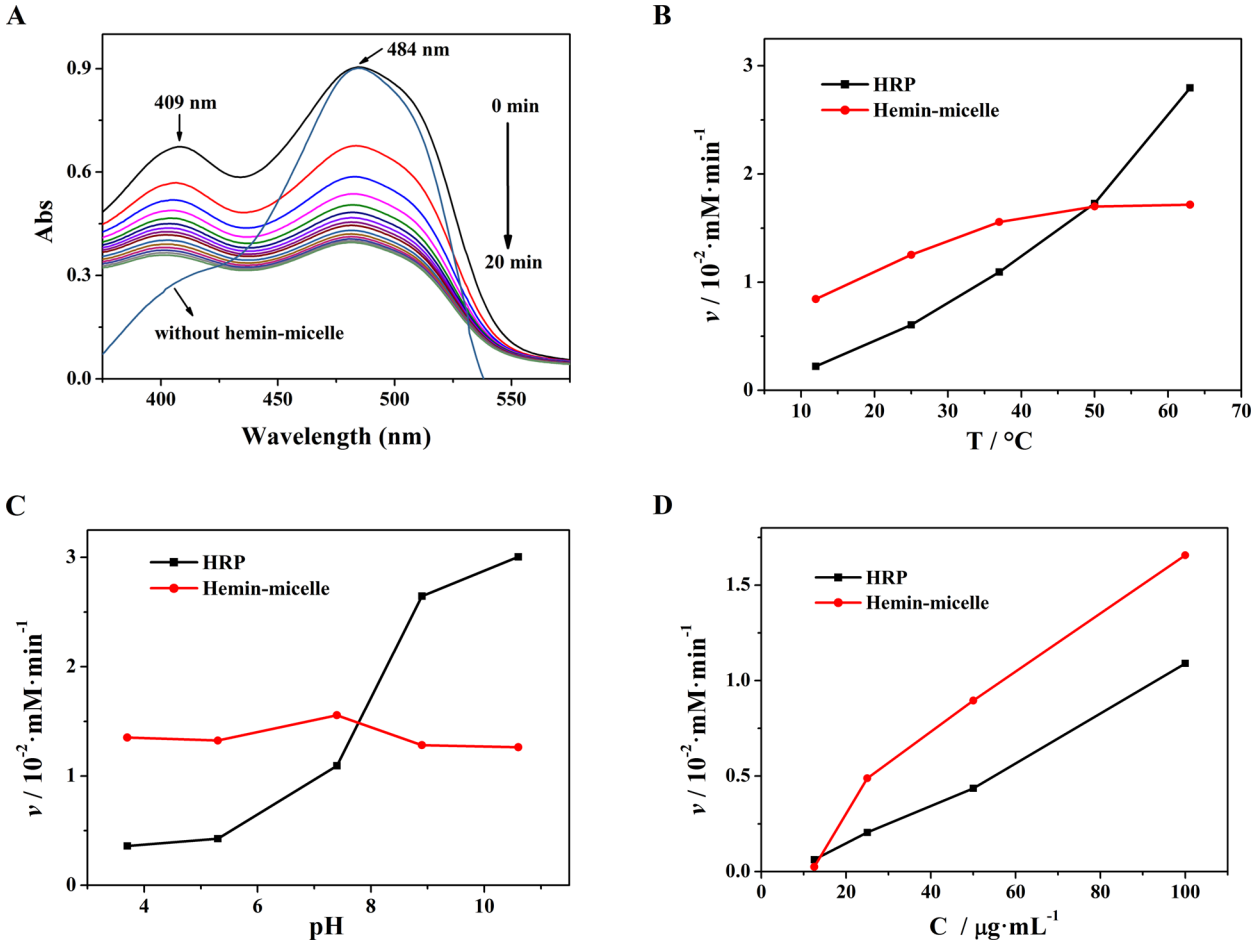

Figure 3. (A) UV−vis spectra of Orange II during the reaction. Initial rates (v) of the degradation reaction catalyzed by hemin-micelle and HRP with temperature, pH and concentration of catalyst as variables: (B) pH 7.4, c = 100 μg/mL, temperature was varied; (C) T = 37 °C, c = 100 μg/mL, pH was varied; (D) pH 7.4, T = 37 °C, concentration of catalyst was varied.

It is well-known that enzymatic activity is dependent on the substrate and the reaction conditions. Therefore, the catalytic activity of the hemin-micelle may be dependent on the pH, temperature, hemin concentration and substrate concentration. The average molar absorption coefficient of Orange II was calculated to be 12.2909 L/(mmol cm) according to the standard curves (see Figure S5 in the Supporting Information). The intensity change of the characteristic absorption peak can be converted to the concentration change of the substrate, and it is further converted to catalytic reaction rate parameters. The catalytic activity was measured through two parameters, namely the initial rate (v) and the conversion rate (Y), within 1 h. Figure 3B-D shows the initial rate (v) of the degradation reaction as being catalyzed by hemin-micelles and HRP with the temperature, pH and concentration of the catalyst as variables. The initial rate of hemin-micelle was higher than that of HRP when the temperature was below 50 °C, or when the pH was below 7.5. The initial rate of hemin-micelle was much less sensitive to the temperature or pH change within the whole range than that of the HRP. The initial rate was dependent on the catalyst concentration, and the higher the concentration, the quicker the initial rate. When the concentration was above 15 μg/mL, the initial rate of hemin-micelle formation was higher than that of HRP. The conversion rate of hemin-micelles was lower than that of HRP, which was the primary drawback of the hemin-micelle in comparison with natural peroxidases (see Figure S6 in the Supporting Information). However, the hemin-micelle conversion was much less sensitive to temperature or pH changes over the whole range. These results demonstrated that the catalytic activity of hemin-micelles was less affected by the temperature and pH changes than natural peroxidases, which exhibited better resistance to the changes in external environment conditions. The effect of the substrate concentration on the catalytic activity of hemin-micelles was also investigated. When the substrate concentration was relatively low, the initial rate sharply increased with increased H_2O_2 or Orange II concentration, and then it gradually slowed down when the concentration went beyond a certain value,

dx.doi.org/10.1021/am505232h | ACS Appl. Mater. Interfaces 2014, 6, 19207−19216

which was also observed for the peroxidase enzyme, as shown in Figure S7 in the Supporting Information.[40]

To investigate the kinetic mechanism underlying the peroxidase-like activity of hemin-micelles, the apparent steady-state kinetic parameters for the peroxidase-like activity were determined by changing the Orange II and H_2O_2 concentrations in this system. Figures S8 and S9 in the Supporting Information show the fitted curves from the Lineweaver–Burk equation of hemin-micelles and HRP. The Michaelis–Menten constant (K_m) and maximum initial velocity (V_{max}) can be obtained from the curves, as shown in Table 1.

Table 1. Apparent Michaelis–Menten Constant (K_m) and Maximum Velocity (V_{max}) of Hemin-Micelles and HRP

catalyst	substrate	K_m (mM)	V_{max} ($\times 10^{-8}$ M s^{-1})
HRP	Orange II	2.93	232.67
	H_2O_2	3.70[a]	8.71[a]
hemin-micelle	Orange II	0.17	64.85
	H_2O_2	2.17	52.62

[a]Data from ref 40.

The smaller the K_m value, the stronger the affinity is between the catalyst and the substrate and the more efficient the catalyst. The apparent K_m values for hemin-micelles with Orange II or H_2O_2 as the substrate were lower than that of HRP, suggesting that hemin-micelles have a higher affinity for Orange II and H_2O_2 than HRP.

The stability is another considerable problem aside from the activity when investigating the performance of a catalyst. Both the micelle and the protein create constitutionally stable scaffolds for hemin, and the hemin can disperse in water at a high concentration. With the natural enzyme, the tertiary structure of protein is easily influenced by extreme environmental conditions, such as high temperature and high pH. The structural change in the protein may reduce the enzyme activity. The block copolymer PEG-*b*-P4VP has a stable chemical structure, which has a certain degree of resistance to high temperatures and high pH values. The thermal stability and pH stability were measured by detecting the concentration change in the catalytic center within 1 h. Table 2 shows the

Table 2. Relative Stabilities of Hemin-Micelles and HRP at Different Temperatures and pH values

		relative stability of the catalytic center (%)	
		hemin-micelle	HRP
T (°C)	50	91.0	89.0
	63	92.5	57.6
	75	75.9	48.3
pH	11	82.8	68.9
	12	89.3	66.9

thermal stability and pH stability of hemin-micelles and HRP. We can see that the hemin-micelle can maintain relatively high stability at the higher temperature, and HRP becomes unstable and loses most of its activity. In an alkaline environment, hemin-micelles have higher stability than HRP, which ensures the activity of the catalyst.

Taken together, these results demonstrate that hemin-micelles retain intrinsic peroxidase-like activities that are the same as natural peroxidases. Hemin-micelles also retain excellent stability against extreme environmental conditions, which is owed to the chemical stability of the block copolymer and the strong coordination interaction between the polymer and the hemin.

3.4. Effect of the Ratio between the Polymer and the Hemin on Catalytic Activity. A group of hemin-micelles were prepared with different mass ratios of polymer to hemin. At higher polymer concentrations (higher R values), the average diameters of the micelles gradually increased (see Figure S10 in the Supporting Information). The UV–vis absorption spectra of the micelles are shown in Figure 4A. The intensity of the absorption peak at 409 nm gradually increased with R changing from 0.5 to 4, which was attributed to the increased loading volume of hemin on the micelle or the change of the coordination state of hemin. The catalytic activity of micelles with different R values was evaluated by using the initial rates and conversions, as shown in Figure 4B. The catalytic activity of micelles decreased with increasing R values.

From the results, we can see that the high polymer concentration may enhance the loading volume of hemin on the micelle, however, the catalytic activity was not correspondingly enhanced. The catalytic center prefers a five coordinate state, which has an open site for the substrate binding, and the high polymer concentration was unfavorable for making adequate contact between the substrate and the catalytic center.[7,27] However, when the mass ratio of PEG-*b*-P4VP to hemin decreases to a lower value, the 4VP moiety is no longer excessive compared with hemin monomer, the loading capacity for hemin would decrease. The block copolymer offers a stable scaffold for the hemin in aqueous media, low polymer concentration would reduce the stability of the hemin-micelle. Considering the factors above, R = 1 was adopted as a reasonable mass ratio of polymer to hemin. In this state, the corresponding mole ratio of 4VP moiety to hemin monomer was 5.5:1, which guaranteed the high loading capacity of hemin-micelle, along with high catalytic activity and high stability.

3.5. Role of Coordination Interaction in the Micelle-Formation Process. To demonstrate the significance of the coordination interaction between pyridine and hemin in the micelle formation process, PEG-*b*-PLys/hemin micelles and PEG-*b*-PCL/hemin micelles were also prepared, and the macro-morphology of the three micelles and their Tyndall phenomena are shown in Figure S11 in the Supporting Information. The three micelles had the same concentrations of block copolymer (100 μg/mL) and hemin (100 μg/mL) before dialysis against the phosphate buffer (pH 7.4).

Regarding the PEG-*b*-PLys/hemin micelle, the self-assembly was driven by electrostatic interactions among the anionic carboxylate groups of hemin and the charged protonated nitrogen atoms of PLys. The micelle was precipitated during the dialysis from an alkaline solution to a phosphate buffer (pH 7.4). The PEG-*b*-PCL/hemin micelle was formed by the hydrophobic interaction between the PCL and the hemin, where there was no coordination interaction. Little precipitate was formed during the dialysis, and most of the hemin was evenly dispersed in solution. Figure S12 in the Supporting Information shows the hydrodynamic diameter distributions of the PEG-*b*-P4VP/hemin micelle and PEG-*b*-PCL/hemin micelle. The PEG-*b*-P4VP/hemin micelles have a smaller diameter and better dispersity than the PEG-*b*-PCL/hemin micelles. We believe that the coordination interaction between the pyridine and the hemin plays an extremely important role

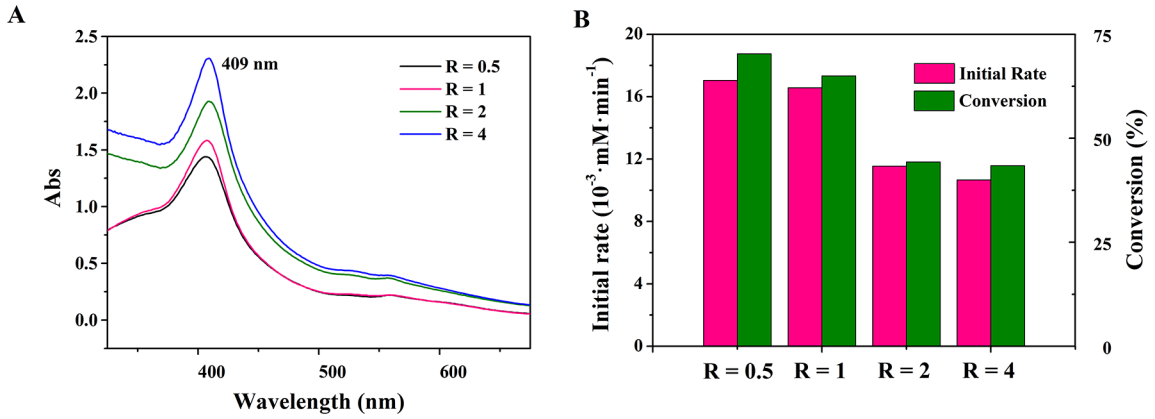

Figure 4. (A) UV−vis absorption spectra of hemin in micelles with different *R* values (*R* = 0.5, 1, 2, and 4). (B) Initial rates and conversions of catalytic systems with different mass ratios of polymer to hemin (*R* value). All samples were prepared in 10 mM phosphate buffer (pH 7.4) and at room temperature.

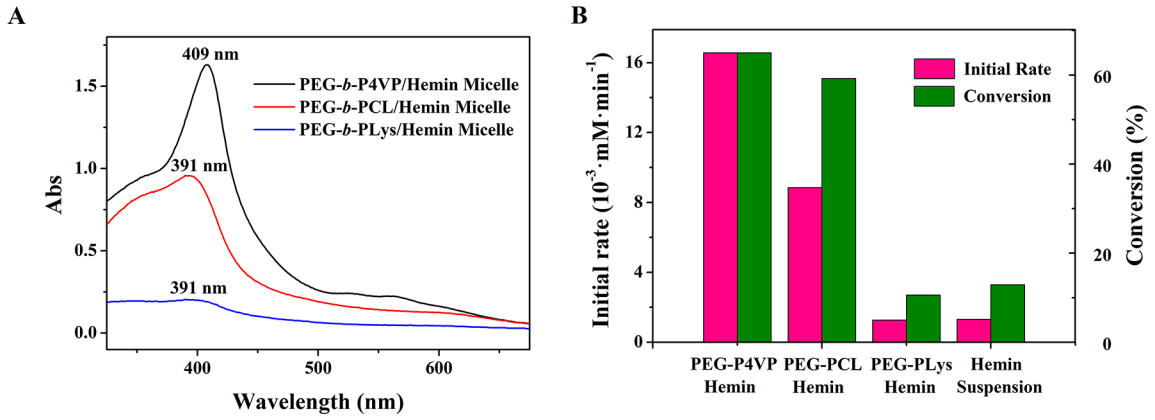

Figure 5. (A) UV−vis spectra of the three micelles. (B) Initial rates and conversions of the three micelles and the hemin suspension. All samples were prepared in 10 mM phosphate buffer (pH 7.4) and at room temperature.

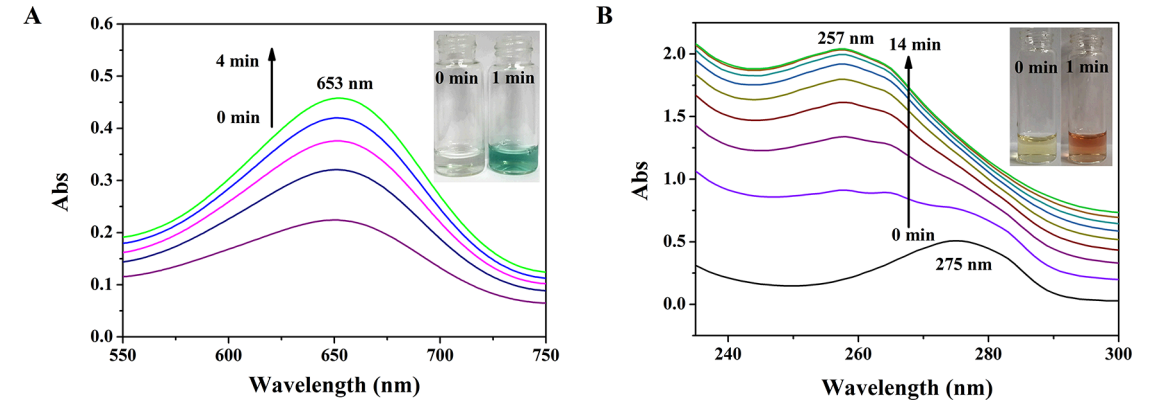

Figure 6. UV−vis spectra and images of colorimetric reactions for (A) TMB and (B) catechol.

in the self-assembly of micelles, and it further influences the catalytic activity.

The UV−vis spectra of PEG-*b*-P4VP/hemin micelles, PEG-*b*-PCL/hemin micelles and PEG-*b*-PLys/hemin micelles are shown in Figure 5A. Regarding PEG-*b*-PLys/hemin micelles and PEG-*b*-PCL/hemin micelles, the Soret band of hemin was 391 nm, indicating the presence of the μ-oxo dimer.[13,35] For PEG-*b*-P4VP/hemin micelles, the Soret band had a red shift to 409 nm because of the coordination interaction between the pyridine and the hemin. The catalytic activity of the three micelles and the hemin suspension in 10 mM phosphate buffer (pH 7.4) were measured by using the initial rates and conversion, as shown in Figure 5B. The PEG-*b*-P4VP/hemin micelles had the best catalytic activity among the three micelles, and they had the highest initial rate and conversion. The PEG-*b*-PLys/hemin complex had almost no catalytic activity because of a failure to self-assemble into micelles. The hemin suspension in 10 mM phosphate buffer (pH 7.4) has poor catalytic activity because of its low solubility and instability in aqueous media and lack of microenvironment for hemin as

dx.doi.org/10.1021/am505232h | *ACS Appl. Mater. Interfaces* 2014, 6, 19207−19216

natural peroxidases. The PEG-*b*-PCL/hemin micelles had a certain degree of catalytic activity, but the hydrophobic interaction failed to inhibit the formation of the μ-oxo dimer, which made it hard to maintain long-term stability.

The analysis above demonstrates that the coordination interaction between hemin and P4VP is particularly important for the high-efficiency self-assembly of hemin-micelles and the enhancement of the catalytic activity. The coordination interaction along with the hydrophobic interaction between the hemin and the P4VP affords a stable composite system with peroxidase-like activity, which mimics the microenvironment of the catalytic center in natural peroxidases to the maximum extent.

3.6. Applications of Hemin-Micelles on Chromogenic Detection and Biocatalysis. 3,3′,5,5′-Tetramethylbenzidine (TMB) is one of the most widely used substrates, and it can react with H_2O_2 when catalyzed by peroxidases and produce a color change.[41−44] Figure 6A shows the UV−vis spectra of TMB solution and the color change. The absorption peak at 652 nm is attributed to the product oxidized TMB. The color of the TMB solution turned blue within 1 min, which indicates the oxidation of TMB by H_2O_2. Phenol is a type of chemical poison, and it is widely used and abundantly produced by modern industry. Phenolic wastewater is an important source of water pollution in the environment, and it causes great harm to human health. Catechol is one type of phenol, and it can be oxidized by H_2O_2 with peroxidases as catalysts along with a clear color change. Hemin-micelles may have similar catalytic activity for phenols as natural peroxidases. Figure 6B shows the UV−vis spectra change of catechol during the oxidation reaction catalyzed by hemin-micelle, along with the color change. The absorption peak at 275 nm is attributed to catechol, which remained unchanged without hemin-micelle. When the H_2O_2 solution was added to the catechol/micelle mixture, the band at 275 nm disappeared gradually, along with the appearance of a new band at 257 nm, which is attributed to the product quinone.

On the basis of the analysis above, hemin-micelles can be used as an efficient detection system for H_2O_2 when it cooperates with some chromogenic substrates. Hemin-micelles have an excellent catalytic ability for the degradation of azo dyes and phenols, which confers great potential for applications in industrial pollutant decontamination. In addition, H_2O_2 is a poisonous product of many biological oxidation processes, for example the oxidation of glucose or alcohol, and the disproportional reaction of reactive oxygen species (ROS), which should be eliminated by peroxidases or catalases. From this point of view, hemin-micelles may have many more applications to multifunctional biocatalysis when cooperating with specific oxidases.[45−51]

4. CONCLUSIONS

Hemin-micelles have been successfully prepared through the self-assembly of PEG-*b*-P4VP and hemin. The micelle serves as an excellent carrier to stabilize hydrophobic hemin in aqueous media and thus enhances the catalytic activity of hemin in the water phase. The coordination interaction between hemin and P4VP facilitates the self-assembly and mimics the microenvironment of heme in natural peroxidases. Compared with natural peroxidases, the artificial peroxidase constructed by the micelle is less costly, easy to prepare and reserve, and has a comparative catalytic activity to that of HRP, or is even higher at stability and has a higher reaction rate. Because of these advantages, hemin-micelles can rival natural peroxidases, and they have potential applications in a variety of simple and cost-effective biosensors. Hemin-micelles also show excellent performance in the removal of dye pollutants or phenols from aqueous solutions in a short time, and thus can be used as a new platform for pollutant decontamination. When the artificial peroxidase cooperates with other enzymes (natural or even artificial) such as alcohol oxidase or superoxide dismutase, the complex artificial enzyme system can perform some supernatural functions, which may become our research interests in the future.

■ ASSOCIATED CONTENT

Ⓢ Supporting Information

Detailed synthetic routes and characterization of block copolymers, the proposed mechanism for the catalytic reaction, fitted equations of the catalytic dynamics, and detailed DLS analysis of the micelles are included here. This material is available free of charge via the Internet at http://pubs.acs.org.

■ AUTHOR INFORMATION

Corresponding Authors

*E-mail: shilinqi@nankai.edu.cn. Fax: +86 22 23503510. Tel: +86 22 23506103 (L.S.).

*E-mail: zyf9182@163.com (Y.Z.).

Notes

The authors declare no competing financial interest.

■ ACKNOWLEDGMENTS

This work was supported by National Natural Science Foundation of China (91127045), the National Basic Research Program of China (973 Program, 2011CB932503), and PCSIRT (IRT1257) for the financial support.

■ REFERENCES

(1) Wolfenden, R.; Snider, M. J. The Depth of Chemical Time and the Power of Enzymes as Catalysts. *Acc. Chem. Res.* **2001**, *34*, 938−945.

(2) Lin, Y.; Ren, J.; Qu, X. Catalytically Active Nanomaterials: A Promising Candidate for Artificial Enzymes. *Acc. Chem. Res.* **2014**, *47*, 1097−1105.

(3) Breslow, R. Biomimetic Chemistry. *Chem. Soc. Rev.* **1972**, *1*, 553−580.

(4) Murakami, Y.; Kikuchi, J.; Hisaeda, Y.; Hayashida, O. Artificial Enzymes. *Chem. Rev.* **1996**, *96*, 721−758.

(5) Dong, Z.; Luo, Q.; Liu, J. Artificial Enzymes Based on Supramolecular Scaffold. *Chem. Soc. Rev.* **2012**, *41*, 7890−7908.

(6) Hamid, M.; Khalil ur, R. Potential Applications of Peroxidases. *Food Chem.* **2009**, *115*, 1177−1186.

(7) Arai, T.; Ishibashi, K.; Tomizaki, K.; Kato, T.; Nishino, N. Slipping of a Histidine Improved the Peroxidase Activity of a De Novo Designed Polypeptide Packing an Iron Porphyrin. *Tetrahedron* **2005**, *61*, 4023−4030.

(8) Zhang, Y.; Xu, C.; Li, B. Self-assembly of Hemin on Carbon Nanotube as Highly Active Peroxidase Mimetic and its Application for Biosensing. *RSC Adv.* **2013**, *3*, 6044−6050.

(9) Nastri, F.; Lista, L.; Ringhieri, P.; Vitale, R.; Faiella, M.; Andreozzi, C.; Travascio, P.; Maglio, O.; Lombardi, A.; Pavone, V. A Heme-Peptide Metalloenzyme Mimetic with Natural Peroxidase-Like Activity. *Chem.—Eur. J.* **2011**, *17*, 4444−4453.

(10) Zhang, F.; Long, X.; Zhang, D.; Sun, Y.; Zhou, Y.; Ma, Y.; Qi, L.; Zhang, X. Layered Double Hydroxide-hemin Nanocomposite as Mimetic Peroxidase and Its Application in Sensing. *Sens. Actuators, B* **2014**, *192*, 150−156.

(11) Guo, Y.; Deng, L.; Li, J.; Guo, S.; Wang, E.; Dong, S. Hemin-Graphene Hybrid Nanosheets with Intrinsic Peroxidase-like Activity for Label-free Colorimetric Detection of Single-Nucleotide Polymorphism. *ACS Nano* **2011**, *5*, 1282−1290.
(12) Xue, T.; Peng, B.; Xue, M.; Zhong, X.; Chiu, C.; Yang, S.; Qu, Y.; Ruan, L.; Jiang, S.; Dubin, S. Integration of Molecular and Enzymatic Catalysts on Graphene for Biomimetic Generation of Antithrombotic Species. *Nat. Commun.* **2014**, *5*, 3200.
(13) Wang, Q.; Yang, Z.; Zhang, X.; Xiao, X.; Chang, C. K.; Xu, B. A Supramolecular-Hydrogel-Encapsulated Hemin as an Artificial Enzyme to Mimic Peroxidase. *Angew. Chem., Int. Ed.* **2007**, *46*, 4285−4289.
(14) Castriciano, M.; Romeo, A.; Baratto, M.; Pogni, R.; Scolaro, L. Supramolecular Mimetic Peroxidase Based on Hemin and PAMAM Dendrimers. *Chem. Commun.* **2008**, *44*, 688−690.
(15) Hu, P.; Han, L.; Dong, S. A Facile One-Pot Method to Synthesize a Polypyrrole/Hemin Nanocomposite and Its Application in Biosensor, Dye Removal, and Photothermal Therapy. *ACS Appl. Mater. Interfaces* **2014**, *6*, 500−506.
(16) Zhang, L.; Eisenberg, A. Multiple Morphologies of "Crew-Cut" Aggregates of Polystyrene-b-poly(acrylic acid) Block Copolymers. *Science* **1995**, *268*, 1728−1731.
(17) Chen, D.; Jiang, M. Strategies for Constructing Polymeric Micelles and Hollow Spheres in Solution via Specific Intermolecular Interactions. *Acc. Chem. Res.* **2005**, *38*, 494−502.
(18) Kataoka, K.; Harada, A.; Nagasaki, Y. Block Copolymer Micelles for Drug Delivery: Design, Characterization and Biological Significance. *Adv. Drug Delivery Rev.* **2012**, *64*, 37−48.
(19) Wang, Y.; Xu, H.; Ma, N.; Wang, Z.; Zhang, X.; Liu, J.; Shen, J. Block Copolymer Micelles as Matrixes for Incorporating Diselenide Compounds: A Model System for a Water-Soluble Glutathione Peroxidase Mimic Fine-Tuned by Ionic Strength. *Langmuir* **2006**, *22*, 5552−5555.
(20) Huang, X.; Dong, Z.; Liu, J.; Mao, S.; Luo, G.; Shen, J. Tellurium-Based Polymeric Surfactants as a Novel Seleno-Enzyme Model with High Activity. *Macromol. Rapid Commun.* **2006**, *27*, 2101−2106.
(21) Yu, S.; Yin, Y.; Zhu, J.; Huang, X.; Luo, Q.; Xu, J.; Shen, J.; Liu, J. A Modulatory Bifunctional Artificial Enzyme with both SOD and GPx Activities Based on a Smart Star-Shaped Pseudo-block Copolymer. *Soft Matter* **2010**, *6*, 5342−5350.
(22) Zhang, Z.; Ma, R.; Shi, L. Cooperative Macromolecular Self-Assembly toward Polymeric Assemblies with Multiple and Bioactive Functions. *Acc. Chem. Res.* **2014**, *47*, 1426−1437.
(23) Xia, J.; Zhang, X.; Matyjaszewski, K. Atom Transfer Radical Polymerization of 4-Vinylpyridine. *Macromolecules* **1999**, *32*, 3531−3533.
(24) Wang, X.; Zhao, L.; Ma, R.; An, Y.; Shi, L. Stability Enhancement of ZnTPPS in Acidic Aqueous Solutions by Polymeric Micelles. *Chem. Commun.* **2010**, *46*, 6560−6562.
(25) Gao, H.; Xiong, J.; Cheng, T.; Liu, J.; Chu, L.; Liu, J.; Ma, R.; Shi, L. In Vivo Biodistribution of Mixed Shell Micelles with Tunable Hydrophilic/Hydrophobic Surface. *Biomacromolecules* **2013**, *14*, 460−467.
(26) Huang, F.; Wang, J.; Qu, A.; Shen, L.; Liu, J.; Liu, J.; Zhang, Z.; An, Y.; Shi, L. Maintenance of Amyloid β Peptide Homeostasis by Artificial Chaperones Based on Mixed-Shell Polymeric Micelles. *Angew. Chem., Int. Ed.* **2014**, *53*, 8985−8990.
(27) Lu, Y.; Berry, S. M.; Pfister, T. D. Engineering Novel Metalloproteins: Design of Metal-Binding Sites into Native Protein Scaffolds. *Chem. Rev.* **2001**, *101*, 3047−3080.
(28) Moosavi-Movahedi, A. A.; Semsarha, F.; Heli, H.; Nazari, K.; Ghourchian, H.; Hong, J.; Hakimelahi, G. H.; Saboury, A. A.; Sefidbakht, Y. Micellar Histidinate Hematin Complex as an Artificial Peroxidase Enzyme Model: Voltammetric and Spectroscopic Investigations. *Colloids Surf., A* **2008**, *320*, 213−221.
(29) Wang, X.; Chai, Z.; Ma, R.; Zhao, L.; Zhang, Z.; An, Y.; Shi, L. Enhancement of the Photostability and Photoactivity of Metallo-meso-5,10,15,20-tetrakis-(4-sulfonatophenyl) Porphyrins by Polymeric Micelles. *J. Colloid Interface Sci.* **2012**, *388*, 80−85.
(30) Chai, Z.; Gao, H.; Ren, J.; An, Y.; Shi, L. MgTPPS/Block Copolymers Complexes for Enhanced Stability and Photoactivity. *RSC Adv.* **2013**, *3*, 18351−18358.
(31) Chai, Z.; Jing, C.; Liu, Y.; An, Y.; Shi, L. Spectroscopic Studies on the Photostability and Photoactivity of Metallo-tetraphenylporphyrin in Micelles. *Colloid Polym. Sci.* **2014**, *292*, 1329−1337.
(32) Kano, K.; Kitagishi, H.; Kodera, M.; Hirota, S. Dioxygen Binding to a Simple Myoglobin Model in Aqueous Solution. *Angew. Chem., Int. Ed.* **2005**, *44*, 435−438.
(33) Watanabe, K.; Kitagishi, H.; Kano, K. Supramolecular Iron Porphyrin/ Cyclodextrin Dimer Complex that Mimics the Functions of Hemoglobin and Methemoglobin. *Angew. Chem., Int. Ed.* **2013**, *52*, 6894−6897.
(34) Sidorov, S. N.; Bronstein, L. M.; Kabachii, Y. A.; Valetsky, P. M.; Soo, P. L.; Maysinger, D.; Eisenberg, A. Influence of Metalation on the Morphologies of Poly(ethylene oxide)-block-poly(4-vinylpyridine) Block Copolymer Micelles. *Langmuir* **2004**, *20*, 3543−3550.
(35) Silver, J.; Lukas, B. Mössbauer Studies on Protoporphyrin IX Iron (III) Solutions. *Inorg. Chim. Acta* **1983**, *78*, 219−224.
(36) Ryabova, E. S.; Dikiy, A.; Hesslein, A. E.; Bjerrum, M. J.; Ciurli, S.; Nordlander, E. Preparation and Reactivity Studies of Synthetic Microperoxidases Containing *b*-type Heme. *J. Biol. Inorg. Chem.* **2004**, *9*, 385−395.
(37) Hitomi, Y.; Hiramatsu, K.; Arakawa, K.; Takeyasu, T.; Hata, M.; Kodera, M. An Iron (III) Tetradentate Monoamido Complex as a Nonheme Iron-based Peroxidase Mimetic. *Dalton Trans.* **2013**, *42*, 12878−12882.
(38) Mutambanengwe, C.; Togo, C.; Whiteley, C. Decolorization and Degradation of Textile Dyes with Biosulfidogenic Hydrogenases. *Biotechnol. Prog.* **2007**, *23*, 1095−1100.
(39) Cordoba, A.; Magario, I.; Ferreira, M. Evaluation of Hematin-catalyzed Orange II Degradation as a Potential Alternative to Horseradish Peroxidase. *Int. Biodeterior. Biodegrad.* **2012**, *73*, 60−72.
(40) Gao, L.; Zhuang, J.; Nie, L.; Zhang, J.; Zhang, Y.; Gu, N.; Wang, T.; Feng, J.; Yang, D.; Perrett, S.; Yan, X. Intrinsic Peroxidase-like Activity of Ferromagnetic Nanoparticles. *Nat. Nanotechnol.* **2007**, *2*, 577−583.
(41) Chen, Y.; Cao, H.; Shi, W.; Liu, H.; Huang, Y. Fe-Co Bimetallic Alloy Nanoparticles as a Highly Active Peroxidase Mimetic and Its Application in Biosensing. *Chem. Commun.* **2013**, *49*, 5013−5015.
(42) Wang, X.; Wu, Q.; Shan, Z.; Huang, Q. BSA-stabilized Au Clusters as Peroxidase Mimetics for Use in Xanthine Detection. *Biosens. Bioelectron.* **2011**, *26*, 3614−3619.
(43) Zhang, J.; Zhang, H.; Du, Z.; Wang, X.; Yu, S.; Jiang, H. Water-stable Metal-organic Frameworks with Intrinsic Peroxidase-like Catalytic Activity as a Colorimetric Biosensing Platform. *Chem. Commun.* **2014**, *50*, 1092−1094.
(44) Chen, Q.; Liu, M.; Zhao, J.; Peng, X.; Chen, X.; Mi, N.; Yin, B.; Li, H.; Zhang, Y.; Yao, S. Water-dispersible Silicon Dots as a Peroxidase Mimetic for the Highly-sensitive Colorimetric Detection of Glucose. *Chem. Commun.* **2014**, *50*, 6771−6774.
(45) Wilner, O. I.; Weizmann, Y.; Gill, R.; Lioubashevski, O.; Freeman, R.; Willner, I. Enzyme Cascades Activated on Topologically Programmed DNA Scaffolds. *Nat. Nanotechnol.* **2009**, *4*, 249−254.
(46) Liu, Y.; Du, J.; Yan, M.; Lau, M.; Hu, J.; Han, H.; Yang, O. O.; Liang, S.; Wei, W.; Wang, H.; Li, J.; Zhu, X.; Shi, L.; Chen, W.; Ji, C.; Lu, Y. Biomimetic Enzyme Nanocomplexes and Their Use as Antidotes and Preventive Measures for Alcohol Intoxication. *Nat. Nanotechnol.* **2013**, *8*, 187−192.
(47) Gao, Y.; Hou, C.; Zhou, L.; Zhang, D.; Zhang, C.; Miao, L.; Wang, L.; Dong, Z.; Luo, Q.; Liu, J. A Dual Enzyme Microgel with High Antioxidant Ability Based on Engineered Seleno-Ferritin and Artificial Superoxide Dismutase. *Macromol. Biosci.* **2013**, *13*, 808−816.
(48) Tanner, P.; Balasubramanian, V.; Palivan, C. G. Aiding Nature's Organelles: Artificial Peroxisomes Play Their Role. *Nano Lett.* **2013**, *13*, 2875−2883.
(49) Zheng, X.; Liu, Q.; Jing, C.; Li, Y.; Li, D.; Luo, W.; Wen, Y.; He, Y.; Huang, Q.; Long, Y.; Fan, C. Catalytic Gold Nanopaticles for

Nanoplasmonic Detection of DNA Hybridization. *Angew. Chem., Int. Ed.* **2011**, *50*, 11994−11998.
(50) Yamada, Y.; Tsung, C. K.; Huang, W.; Huo, Z. Y.; Habas, S. E.; Soejima, T.; Aliaga, C. E.; Somorjai, G. A.; Yang, P. D. Nanocrystal Bilayer for Tandem Catalysis. *Nat. Chem.* **2011**, *3*, 372−376.
(51) Shi, J.; Zhang, L.; Jiang, Z. Facile Construction of Multi-compartment Multienzyme System through Layer-by-Layer Self-Assembly and Biomimetic Mineralization. *ACS Appl. Mater. Interfaces* **2011**, *3*, 881−889.